Insight from molecular dynamics simulations on the crystallization tendency of indomethacin polymorphs in the undercooled liquid state

Joseph Gerges, Frederic Affouard

Insight from molecular dynamics simulations on the crystallization tendency of indomethacin polymorphs in the undercooled liquid state

J. Gerges, F. Affouard

Univ. Lille, CNRS, INRA, ENSCL, UMR 8207 - UMET - Unité Matériaux et Transformations, F-59000 Lille, France

ABSTRACT: The crystallization tendency of two crystalline polymorphs of indomethacin (I_α, I_γ) in the undercooled melt has been investigated using molecular dynamics (MD) simulations. The main thermodynamical and dynamical physical parameters involved in the nucleation and growth processes have been determined. A careful attention has been given to the crystal-liquid interfacial free energy which remains really challenging to determine from experiments. The present work particularly sheds the light on the importance of the interplay between the solid-liquid interfacial free energy and the driving force for crystallization. The nucleation and the growth rates have been also estimated in the framework of the classical nucleation theory (CNT) and some growth modes (normal mode, two-dimensional nucleation, and screw dislocation).

INTRODUCTION

The vast majority of drugs - active pharmaceutical ingredients (API) and excipients - are generally prepared in the solid state (powder, tablets, capsules) which can exist in multiple crystalline or amorphous physical forms, having fundamental different physical properties (solubility, stability, mobility) [1]. Until now, drugs have been developed especially in the most thermodynamically stable crystalline state to reach an appropriate long-term storage. However, this state may often exhibit inadequate solubility or dissolution rate resulting in poor bioavailability, particularly for poorly water soluble compounds. In order to overcome these limitations, formulation in the amorphous state has been considered as a suitable solution[2]. However, the amorphous state intrinsically lacks in stability and an eventual recrystallization upon storage could be expected that would obviously negate advantages of using the amorphous state. Furthermore, obtaining the amorphous state itself and thus avoiding crystallization could be also challenging because of the poor glass-forming ability of some pharmaceuticals [1].

Hence, the understanding of the crystallization mechanism in the deeply undercooled liquids is crucial for the development of amorphous materials especially in the drug industry[3]. Significant importance has been given to understand the tendency of a certain material to crystallize, vitrify or recrystallize; but this tendency remains poorly understood[4-6]. The crystallization from the undercooled melt involves complex phenomena which are roughly described as a two-step process i.e. nucleation and growth. Nucleation is the first step in which small crystalline aggregates having a certain critical size randomly form in the amorphous state. Nucleation has

particularly attracted a considerable attention in the framework of the classical nucleation theory (CNT) which remains one of the simplest and most widely used theories that describe nucleation process despite serious limitations in some cases[7-11]. Nucleation is characterized by the so-called nucleation rate N that measures the number of crystalline nuclei formed per unit of volume per unit of time (unit: $m^{-3}.s^{-1}$). Growth is the second step in which the supercritical nuclei may expand[7-12] and it is described by the so-called growth rate G i.e. the rate (unit $m.s^{-1}$) at which the size of the crystalline aggregate increases. Despite their own fundamental specificities, nucleation and growth phenomena actually share three common major physical parameters: the Gibbs free energy difference between the crystal and its melt (the driving force) ΔG, the diffusivity D of the molecules in the liquid state and the crystal-melt interfacial free energy γ [13]. The first two physical parameters ΔG and D are easily obtained experimentally. For example ΔG can be approximated using Turnbull or Hoffman equations[14,15] and D can be replaced by the more accessible experimentally shear viscosity $D \sim \eta^{-1}$ assuming the validity of the Stokes-Einstein relation even though its use is questionable due to a possible decoupling between viscosity and diffusion[9,16]. The third and the more complex parameter is the crystal-melt interfacial free energy γ for which the direct experimental determination, without assumption based on CNT, remains a major problem. This difficulty really contrasts with the "ease" concerning the determination of the fluid-fluid interfacial free energy for which experimental and computational techniques are well established.[17] Despite its importance in the physical description of the crystal morphology or the nucleation rate, only a few experimental data of γ are actually available in the literature and mostly for metallic alloys. Data for molecular compounds are even scarcer.[8,18,19] The experimentally determined values may also differ considerably depending on the specific technique used.[20,21] Simulations thus present a clear interest but they also remain very challenging.[22-25] In recent years, two main approaches based on molecular dynamics (MD) simulation has been frequently employed: the "adiabatic cleaving method (ACM)" proposed by Broughton and Gilmer[26] and the "capillary fluctuation method (CFM)" proposed Hoyt, Asta, and Karma[27,28]. Both have been extended and validated on simple systems composed of hard spheres, Lennard-Jones particles, metal atoms or more rarely of small molecules. The ACM method is based on the fact that the free energy of interface is a thermodynamic state function. One thus may calculate the reversible work required to create a solid-liquid interface i.e the interfacial free energy. ACM involves several steps in which bulk phases (liquid and crystal) are cleaved and rearranged to give interface of interest. The free energy of interface is obtained by a thermodynamic integration in the different steps. This approach has been employed on different simple systems by Davidchack and Laird.[29,30] Recently, it was also used by Handel et al[31] to calculate the ice-water interfacial free energy. In the CFM, the fluctuation of the position of the crystal-liquid interface is used as a measure of its roughness in order to determine its stiffness - soft interface have more fluctuations – which can be directly correlated to the interfacial free energy in the framework of the capillary waves theory. CFM was successfully validated in recent years for monatomic[32] and binary atomic simple systems[33] and more realistic models such as metallic compounds[24,34], alloys[35] and molecular materials such as succinonitrile.[36] Recently, CFM was also used by the authors to estimate the interfacial free energy of nifedipine and felodipine polymorphs.[37] Both ACM and CFM show marked advantages and disadvantages. ACM is usually considered as more precise than CFM to obtain the solid-liquid interfacial free energy γ but it is less precise to measure the anisotropy in γ. ACM requires systems of relatively small sizes made of about N = 10 000 atoms while for CFM simulations larger systems are necessary of about 50 000 to 100 000 atoms.

ACM numerical implementation is more complex since it entails following a rather cumbersome thermodynamic route requiring many different simulations while only one (but extensive) simulation is necessary in CFM in order to get the interface fluctuations. In addition, great care must be taken in the construction of cleaving potential in ACM for molecular systems. A major issue in CFM is the definition of a local parameter at the molecular scale that can distinguish between the liquid and the solid phases in order to obtain precisely the position of the interface.[25,28,34,38] In addition, the interface is intrinsically treated as "rough" in CFM. Both ACM and CFM approaches actually provide γ at the melting temperature at which liquid and crystal are at equilibrium. It should be noted that other promising methods have been also proposed based on mold integration[39], umbrella sampling method[40], seeding[41], metadynamics[42], or tethered Monte Carlo[43] but they have only been applied on simple model systems so far.

Indomethacin (see Figure 1) is a non-steroidal, anti-inflammatory agent with anti-pyretic and analgesic properties[44] used as a prescription medication to reduce fever, pain and swelling. It is a hydrophobic poorly water soluble drug[45], which makes it a subject to many studies[8,46,47]. This system is particularly interesting due to its rich polymorphism and the availability of experimental data[3,8,45,48,49]. Indomethacin exhibits a monotropic system that has two structurally solved polymorphs: α (I_α) and γ (I_γ) forms[49]. I_γ has the highest melting temperature $T_m \approx 434$ K[8,45] with a density of 1.38 g/cm^3 [50] (at 300 K) and is the most thermodynamically stable polymorph[44] while I_α has a melting temperature of $T_m \approx 428$ K[8] with a density of 1.40g/cm^3 [50] (at 300 K). This monotropic system thus presents an unusual inversion between stability and density in which the metastable form, I_α, has a higher density than the stable form, I_γ. This inversion is attributed to the local hydrogen bonding (HB) organization of the molecules of each polymorph. The molecules of I_γ form dimers by linking their carboxylic groups with hydrogen bonds while the molecules of I_α form trimers with two molecules linked via their carboxylic groups by hydrogen bonds and the third molecule linked via its carboxylic group to the ketone group of the closest neighbor. This supplementary hydrogen bond causes a more compact crystalline arrangement and thus I_α presents a higher density than I_γ. These differences limit the chemical activity of the less dense phase[8,51]. Those two polymorphs crystallize from the melt: I_γ have been reported to crystallize close and below the glass transition temperature $T_g \approx 315$ K while at higher temperatures, the formation of I_α is predominant[8,50]. A third polymorph was also mentioned in literature (δ)[3]; it was reported with a sample crystallized from a methanol solution. Andronis and Zografi[8] determined the nucleation rate N and the growth rate G of I_α and I_γ polymorphs from the melt of a purified I_α crystal. The temperature range was from 293 K to 373 K where two different morphologies were encountered: a needle like grow for I_γ and compact spherules grow for I_α. The behavior of the growth was found to be favorable of a two dimensional growth[3,8] since indomethacin has a high entropy of fusion (~11 R) where this model of growth is applicable to similar materials[8,9,13]. These determinations were made just at a small range of temperatures near T_g and the model assumes that $D \sim \eta^{-1}$ represents accurately the effect of the mobility which is not always the case [9,16]. Thus, the choice of the viscosity as a replacement of the diffusivity may have an impact on the overall nucleation and growth rates. It was also mentioned that additional investigations are needed to fully understand the crystallization process of I_γ since its crystallization is not consistent with what was shown in too many materials where the maximum of the nucleation rate is located above T_g and the maximum of the growth rate is found at a higher temperature often close to the melting temperature. Wu and Yu[3] studied the crystallization from a melt of γ indomethacin for temperature ranging from

323 K to 423 K. They found that I_α and I_γ grow in different morphologies as function of temperature. At high temperatures ($T>T_g$+19 K) polycrystalline growth was observed and at low temperatures ($T<T_g$+19K) a randomly oriented fibers were detected. Wu and Yu[3] were also able to precisely obtain the growth rate G of both polymorph, I_α and I_γ, from the melt. Oppositely to the Andronis and Zografi[8] works, they have shown that a simple continuous growth may well reproduced the experimental data taking into consideration the break-down of the Stokes-Einstein relation and replacing $D\sim\eta^{-1}$ by its fractional variant $D\sim\eta^{-\xi}$.

In this study, we used the available theories of nucleation (CNT) and growth (continuous growth, growth by two dimensional nucleation and the growth originating from screw dislocation) combined with the direct calculation of all relevant parameters (ΔG, D and γ) using molecular dynamics (MD) simulation to investigate the conditions that will favor crystallization/vitrification of indomethacin polymorphs. While the driving force ΔG and the diffusion coefficient D are quite accessible from MD simulations, the solid-liquid interfacial free energy is a difficult parameter to compute [20,52] and only few data for molecular systems do exist [8,18,19,36]. The important role of this parameter was discussed in several studies[22,53-55] and its calculation for the indomethacin polymorphs was one of the main motivations for this work. The solid-liquid interfacial free energy γ was estimated for both polymorphs using the capillary fluctuation method which proved its validity to similar systems[37]. Those calculations, accompanied with guidance from the available theories on nucleation and growth, allowed us to observe the relative importance of each parameter during the phase transformation. This study also allowed us to explore the conditions that might favor the crystallization or the vitrification of low molecular weight systems in a more general approach.

SIMULATIONS DETAILS

In this section, we will summarize the essential steps used to calculate the different physical parameters relevant for nucleation and growth processes. Additional details can be found in reference[37].

The DL_POLY package[56] and the force field OPLS[57] were used to perform Molecular dynamics (MD) simulations. The OPLS force field was chosen due to its recognized capability of reproducing "reasonably well" some experimental data (density, enthalpy of vaporization, heat capacities, surface tension, dielectric constant, volumetric expansion coefficient, isothermal compressibility, mixing free energy) for a large number of molecules with low molecular weight. A few benchmarks have been reported in the literature[58-60] in which the accuracy of the OPLS force field was extensively tested including some tests over a broad range of temperatures.

NPT or NVT statistical ensembles were employed during the different simulation runs where N is the number of molecules, P the pressure, T the temperature and V the volume. N is constant in all simulations and Berendsen barostat and thermostat were applied to control the pressure and temperature respectively. Atmospheric pressure was used in all NPT simulations. At the end of each NPT run, the volume after equilibration was utilized for successive NVT simulations. The integration of Newton's equation of motion was made with a time step of 0.001 ps. Van der Waals interactions were calculated with a cutoff radius of 10 Å. The calculation of the long

range electrostatic interactions was done using Ewald summation with the same cutoff radius. Periodic boundary conditions were applied in all directions.

The crystallographic data for both indomethacin polymorphs was taken from the Cambridge Crystallographic Data Center[61]. Small simulation boxes (of about N = 100 molecules) were used in order to perform MD simulations to estimate the density of the crystal $\rho_{cx}(T)$ and its enthalpy $H_{cx}(T)$ at different temperatures from 100 K to 700 K upon heating. At high temperature the melting occurs which is detected by the sudden drop of the density. Then, subsequent MD simulations were realized from 700 K to 100 K in order to obtain the density of the liquid $\rho_{lq}(T)$ and its enthalpy $H_{lq}(T)$. Some density results are reported in Table 1 for which a fair agreement is found with respect to experimental data. The detailed calculation of $\Delta H(T) = H_{lq}(T) - H_{cx}(T)$ used in the following is provided as supplementary material (see figure S1). The diffusion coefficient is obtained by first equilibrating the melted system for 1 ns in a NPT ensemble followed by a 3 ns run in the NVT ensemble for each temperature. The NVT runs enabled us to obtain the diffusion coefficient D by calculating the mean square displacement$< r^2(t) >$ which was fitted afterwards using the linear relation $< r^2(t) >= 6Dt$. The shear viscosity η was also computed from the stress-stress autocorrelation functions using the Green-Kubo relations[62] in order to check the ability of the force field to represent with enough accuracy the transport properties of indomethacin (see Fig. 2).

Solid-liquid coexistence simulations [63-67] were performed on large boxes (of about N = 4800 molecules) to estimate the melting temperature T_m. Liquid and crystal systems were first separately equilibrated at an estimated melting temperature (basically the experimental melting temperature) using the NPT ensemble. Then, the two systems were combined and equilibrated to generate a bi-phasic system (see Figure 3). Finally the biphasic system is simulated at different temperatures above and below the experimental melting temperature. The density of the system is thus monitored enabling the detection of T_m i.e. the temperature where the density remains stable is considered as the melting temperature. An example of plot density vs. temperature is provided as supplementary material (figure S2). A comparison of some experimental and simulated melting temperatures can be found in Table 1. The melting enthalpy was also obtained by the enthalpy difference between the crystal and the liquid which was extracted from the MD simulation results. Both experimental and simulated melting enthalpies are reported in Table 1. Overall, a fair agreement is found between simulations and experimental data. The agreement is particularly good for densities (~4%), melting temperatures (~2%) and the melting enthalpy of the I_γ form (below 1%). For the melting enthalpy of the I_α form the disagreement is a bit more important (~12%) but it remains acceptable.

The capillary fluctuation method (CFM)[30,38,70-72] has been used in the present work to calculate the crystal-liquid interfacial free energy. CFM was actually selected since it requires only one (but extensive) simulation compared to some other approaches such as the "adiabatic cleaving method" for which many different simulations are necessary. Another reason which has motivated the choice of CFM originates from several successful tests of this method for molecular systems [68] including nifedipine and felodipine by the authors [37]. In addition, CFM also offers the possibility to study in details the impact of the anisotropy (future works).

CFM requires the simulation of the interface in equilibrium at the melting point and the calculation of the fluctuations of the position of the crystal-liquid interface $h(x)$. The fluctuations are then Fourier transformed. The power spectrum of a quasi-one-dimensional interface can be thus written as:

$$< |h(q)|^2 >= \frac{k_B T_m}{L_X L_Z \tilde{\gamma}_m q^2} \quad (1)$$

where $h(q)$ is the one dimensional Fourier transform of $h(x)$ with q as the wave number, the symbol $<>$ represents the time average, k_B is the Boltzman constant. L_Z and L_X are the thickness and the width of the simulation box respectively where $L_Z \ll L_X$ in order to obtain a quasi-one-dimensional interface (see Fig. 3).

The interfacial stiffness $\tilde{\gamma}_m$ will be considered as a fair estimation of the interfacial free energy γ_m neglecting the effect of the anisotropy of the interfacial free energy. The latter was shown to be relatively weak in many studies performed on metals, alloys or small organic molecules.[28,33,34,36,69,70] However, these systems possess relatively high symmetry in the crystal structures and components are much less complex than the pharmaceutical Indomethacin molecule. Face anisotropy is expected for organic molecules where different functional groups may be exposed at difference crystal faces, and there have been plenty of examples demonstrating their effects on crystal growth rates and the resulted morphological differences.[71] Therefore, the anisotropy of interfacial free energy might possibly be important for Indomethacin and this issue clearly deserves additional extensive studies. In addition, the crystal face chosen in this work which is in contact with the liquid possesses about the same planar density of molecules for both polymorphs (2.0 x 10^{-2} molecules/Å^2) which makes the comparison of the interfacial free energies of I_α and I_γ possible.

The same biphasic (crystal-liquid) simulation box employed to estimate the melting temperatures was used to calculate γ_m (see Figure 3). For the two polymorphs, the crystalline box is orientated such as the direction Y normal to the interface is parallel to the vector $\vec{b}$ of the crystalline cell and the direction along the interface X is parallel to the direction $\vec{a}$. A NVT run for 600 ps was done where the configurations of the last 5000 configurations were stored for data analysis. Two interfaces were thus created due to boundary conditions and the profile of each interface is described by a function $h(x)$. Figure 3a shows the biphasic system used to determine the crystal-liquid interfacial free energy of I_α as an example. A rotational-invariant order parameter [24,38,72-75], which relies on spherical harmonics, was used to determine the interface position. It allowed the discrimination between liquid-like and solid like molecules. Figure 3b shows the evolution of ϕ along the direction perpendicular to the interface (y direction). The crystal and the liquid domains are clearly showed in this figure enabling us to locate the interface i.e. the molecules that have an intermediate value $0.06 < \phi < 0.15$ are considered as interfacial molecules. The intercept of the plots of $ln(< |h(q)|^2)$ versus $ln(q)$ permitted the estimation of the value of the interfacial free energy. The linear behavior of $ln(< |h(q)|^2 >)$ as function of $ln(q)$ at small q where Eq. 1 is valid[28], is an indicator of the roughness of the interface[69]. It is shown in Figure 4 for both polymorphs of indomethacin. The values of the interfacial free energies of I_α and I_γ are given in Table 1.

RESULTS AND DISCUSSION

In this section, the results obtained from MD simulations for the different thermodynamic factors i.e the driving force for crystallization, the crystal-liquid interfacial free energy as well as the coefficient of diffusion will be presented. Then, the crystallization tendency of the two investigated polymorphs will be discussed in the framework of the classical models used to describe the homogenous nucleation and growth.

Diffusion coefficient and driving force for crystallization

Figure 2 shows the diffusivity D (in inset) and the shear viscosity η of indomethacin in the equilibrated liquid state as a function of temperature T. Upon cooling, D and η deviate from the Arrhenius behavior which is a typical behavior of fragile glass-formers[76]. Figure 2 shows that the present MD simulations provide a reasonable agreement between the simulated and the experimental viscosity[8,77]. The MYEGA equation proposed in ref. [78] was used in this work to fit the transport properties as a function of temperature. In contrast to the most frequently used Vogel-Tamman-Fulcher (VFT) equation[76], the MYEGA equation[78] was shown to provide accurate description of dynamics over a broader range of temperatures [79]. Hence, the fitting procedure allows estimating the values of the diffusivity D below the melting temperature which is an essential requirement to calculate the pre-factor of the CNT. The agreement between the extrapolated value of the diffusion coefficient obtained from the present MD simulations with the experimental values obtained by Swallen et al.[48] close to the glass transition temperature demonstrates the validity of the approach (see Fig. 2). However, the extrapolation of both the calculated D(T) and shear viscosity η(T) seems to indicate that the molecular dynamics in simulation is slower than experiments. This difference could originate from the OPLS force field as reported in a recent benchmark performed on glycerol in ref.[59] in which shows a similar trend was reported. As a final remark, it should be noted that in the present high temperature regime investigated from MD simulations (see Figure 2), the Stokes-Einstein relation holds relatively well (see supplementary material Figure S3) although a breakdown of this relation has been reported by Wu and Yu[3] in the deep undercooled regime.

The Hoffman equation[15] was used to calculate the Gibbs free energy difference ΔG between the crystal and the liquid states as a function of temperature for I_α and I_γ. It is given by:

$$\Delta G = \Delta H_m \frac{(T_m - T)T}{T_m^2} \quad (2)$$

where ΔH_m and T_m are the melting enthalpy and temperature respectively (see previous section). The Hoffman equation[15] has been found to predict accurately ΔG for small molecular weight glass formers [80,81]. The evolution of ΔG as function of temperature shows clearly that the system is monotropic as found experimentally[50], where the γ-form has a higher ΔG and thus it is the stable phase even though its density is lower (see Table 1 and Figure S4 in supplementary material). As expected, a slight disagreement is observed while comparing the simulated and experimental ΔG data. This disagreement is due to the differences between the experimental and the simulated ΔH_m & T_m (see Table 1).

Solid-liquid interfacial free energy

The interfacial free energies at the melting temperature γ_m computed by the capillary fluctuation method were found to be 27 $\pm$ 3 mJ/m^2 for I_γ and 22 $\pm$ 3 mJ/m^2 for I_α. Interfacial free energies have been also obtained experimentally by Andronis et Zografi[8] and make possible a potential comparison with the values obtained numerically in the present investigation (see Figure 5). The experimental values obtained were about 16.5 – 18.5 mJ/m^2 for the stable I_γ polymorph and about 16.2 – 16.8 mJ/m^2 for the metastable I_α polymorph. To the knowledge of the authors, indomethacin is the only pharmaceutical compound for which the solid-liquid interfacial free energy has been experimentally determined and, more generally, experimental data are really scarce for molecular compounds[8,18,19]. Overall, both numerical and experimental data are of the same order. Interestingly, they show a similar trend: the solid-liquid interfacial free energy for I_γ and I_α polymorphs are close but the value of metastable phase I_α is found a bit lower.

In the present case, a direct comparison of the interfacial free energy values determined from experiments and simulations is intrinsically difficult for two main reasons:

- From experiments, the interfacial free energy is actually indirectly obtained by Andronis et Zografi[8] by fitting the expression of the nucleation rate as predicted by CNT to the experimental nucleation rate. So, the validity of CNT is fully assumed in this approach. In other words, the interfacial free energy is thus taken as a fitting parameter assuming the validity of CNT and not directly measured. Furthermore, the range of temperatures considered to perform this fitting procedure is close to the temperature at which the nucleation rate reaches its maximum .i.e. in the undercooled regime about 100 K below the melting temperature T_m. It is the temperature range where nucleation is actually observed experimentally (see nucleation rate in Figure 6).

- From simulations, the interfacial free energy is directly calculated based on the capillary fluctuations technique without assumption on the validity of CNT. However, the calculation using the employed method can be only done at the melting temperature T_m at which the crystal-liquid interface is at equilibrium.

An indirect comparison is possible either by extrapolating numerical data to lower temperatures or experimental data to higher temperatures (see supplementary material Figure S5). However, both types of extrapolation possess a few flaws requiring some approximations and assumptions. The possible temperature-dependence of the solid-liquid interfacial free energy $\gamma(T)$ have been discussed in several works [82] and the need to use an effective temperature dependent interfacial free energy has been shown from MD simulations to reproduce nucleation rates in the framework of the CNT [83-89]. Hence, it was suggested that the interfacial free energy could increase with T[23] and an arbitrary equation has been in proposed in [84] inspired from the Turnbull law [14] for the temperature dependent interfacial free energy $\gamma(T)$:

$$\gamma(T) = \gamma_m \cdot \left[\frac{\rho_{cx}(T)}{\rho_{cx}(T_m)}\right]^{2/3} \cdot \left[\frac{\Delta H(T)}{\Delta H_m}\right] \quad (3)$$

where $\Delta H(T)$ is the enthalpy difference between the solid and the liquid as a function of temperature. The detailed calculation of $\Delta H(T)$ is provided as supplementary materials (see figure S2).The mathematical form of equation 3 is arbitrary but a major contribution of entropy

(neg-entropic model[90,91]) to the interfacial free energy is intrinsically assumed: the interfacial free energy necessary decreases upon decreasing temperature i.e. the slope of equation 3 is always positive. Assuming the validity of this equation and based on the calculated values of the density and enthalpy (see previous section and Table 1), the solid-liquid interfacial free energy has been estimated as function of the temperature and it is shown in Figure 5. This figure clearly shows that the difference between the theoretical and experimental values of the interfacial free energy could be drastically reduced taking into consideration the temperature dependence of γ. Although a major role of entropy seems very reasonable and validated by many studies[90,91], it should be mentioned that the necessary positive slope of Equation 3 is clearly a strong limitation in the present work.

The extrapolation of experimental data to higher temperatures has been also performed by Andronis et Zografi[8] (See Figure 11 in ref.[8] or supplementary material Figure S5). The temperature dependence of the interfacial free energy was fitted using some adjustable parameters by a straight line with a slope that could be either positive or negative. The extrapolation of experimental data to higher temperatures and the extrapolation of numerical data to lower temperatures actually are in very reasonable agreement for the I_γ polymorph. This similar trend reinforces the confidence in the obtained results for the I_γ polymorph. However, experimental and simulation data give opposite slopes for the interfacial free energy temperature-dependence of $\gamma(T)$ for the I_α polymorph. At this stage, the authors have no clear explanation to explain this disagreement between simulation and experiment since both types of extrapolations (see above) could be actually questioned. It should be noted that while the fit performed Andronis et Zografi[8] (See Figure 11 in ref.[8] or supplementary material Figure S5) seems reasonable for the I_γ polymorph (i.e. an increase of the interfacial free energy upon increasing temperature – positive slope), it is more questionable for the I_α polymorph. Data for the I_α polymorph are actually very close to each other's. Except the first point at the lowest temperature, the remaining three points suggest a positive slope. In their paper, Andronis et wrote "… the value of the interfacial free energy for the alpha-crystal form is fairly constant and very similar for the two procedures". Another procedure used by Andronis et Zografi[8] (see figure 10 in ref.[8]) suggests a constant value ~ 17 mJ/m2 for the I_α polymorph.

Owing the large uncertainties of both numerical of experimental approaches and extrapolation, a direct comparison does not seem very meaningful. Although numerical and experimental interfacial free energy does not match exactly, both data interestingly show that the solid-liquid interfacial free energy for the metastable phase I_α is a bit lower than for the stable I_γ polymorph. Indeed, a lower value for the metastable form with respect to the stable form is expected since at the crystal-liquid interface, the surface of a less stable phase is likely to be more disordered than the surface of a most stable one, hence the interfacial free energy is likely to be smaller. This trend is also well in line with the well-known Ostwald rule of stage [92] suggesting that the crystal phase that nucleates is not the most thermodynamically stable phase but rather another metastable phase that is closest in Gibbs free energy to the parent phase. Moreover, this tendency is consistent with the melting entropy $\Delta S_m = \Delta H_m / T_m$ of both polymorphs. ΔS_m =75.9 and 90.6 J.mol^{-1}K^{-1} for the metastable form I_α and the stable form I_γ respectively (see Table 1). From simulations, the same trend is found and $\Delta S_m = 68.1$ and 92.7 J.mol^{-1}K^{-1} can be calculated for I_α and I_γ (see Table 1).

As indicated in the simulation details section, the anisotropy of the interfacial free energy was not considered in the present study. Although previous studies[28,33,34,36,69,70] have shown that anisotropy is relatively weak, it could be a significant issue since Indomethacin is more dissimilar than the simple systems for which anisotropy has been studied (metals, alloys, simple molecules) so far. [28,33,34,36,69,70] Nevertheless, it should be reminded that even a small anisotropy difference of about 1%–4% in the interfacial free energy is sufficient to have a very strong impact on crystallization as observed on dendrite shapes. [68] Using the obtained values in the present work (22±3 and 27±3 mJ/m^2 for the I_α and I_γ polymorph respectively), a few % difference would be below the uncertainties ±3 mJ/m^2 of the CFM employed here and thus not really conclusive. The anisotropy of interfacial free energy of Indomethacin could be also be much more important than a few % but it seems unlikely based on the reported experimental information on Indomethacin crystallization at least in some temperature ranges above T_g. Indeed, Wu and Yu[3] have investigated in details crystal growth of Indomethacin polymorphs which actually possess some interesting specificities. It was particularly reported that above T_g + 19 K both I_α and I_γ polymorphs similarly grow as largely randomly oriented crystalline clusters with a similar growth rate mostly controlled by diffusion (as also observed in the present MD investigation). Therefore, it seems that above T_g + 19 K, at least, the growth rates are not associated with a specific crystallographic direction and the crystalline face anisotropy does not thus seem to play a major role for growth. However, below T_g + 19 K, the situation is clearly changing and Indomethacin polymorphs grow differently with a sudden rise of growth near T_g. Interestingly, in this situation, Indomethacin polymorphs are found to grow with a preferred crystallographic direction which is different for each polymorph. These new modes of growth with different kinetics close to T_g are poorly understood but seem clearly influenced with the crystal structures and interfaces. Nevertheless, a closer examination of Figure 3 in Wu and Yu[3] shows that close to T_g, the growth rate of the I_α polymorph is about one decade higher than for the I_γ polymorph which is at first glance consistent with its lower interfacial free energy as obtained in the present paper and the Andronis et Zografi[8] work.

Nucleation and growth rates

Once all the parameters involved in the nucleation mechanism and their temperature dependencies are obtained from MD simulations (see above), the steady-state nucleation rate N can be estimated using the following expression based on CNT:

$$N = A_N(T) \cdot exp\left[-\frac{\Delta G^*}{k_b T}\right] \quad (4)$$

where $A_N(T)$ is the kinetic pre-factor, $\Delta G^* = \frac{16\pi}{3}\left[\frac{\gamma^3}{\Delta G_v^2}\right]$ the nucleation barrier and ΔG_v is the Gibbs free energy difference per unit volume between crystal and liquid states. The pre-factor is expressed as $A_N(T) = Z \cdot n_{lq} \cdot \frac{24\mathrm{D}n^{*\frac{2}{3}}}{\lambda^2}$ where $\lambda = 1/{n_{lq}}^{1/3}$ is the atomic jump distance, $n^* = (4/3)(\pi r^{*3} n_{cx})$ is the number of atoms in the critical nucleus, $r^* = 2\gamma/\Delta G_v$ is the critical radius of the nucleus, n_{lq} and n_{cx} are the number density of the liquid and the crystal respectively and $Z = (\Delta G_v/6\pi k_B T n^* n_{cx})^{1/2}$ is the Zeldovich factor.[93]

The steady state nucleation rate N as function of the temperature T for the two investigated polymorphs I_γ and I_α is shown in Figure 6a. The expected bell-shaped behavior was obtained. This is due to the decrease of the mobility and the increase of the Gibbs free energy difference between the crystal and the liquid upon cooling. While the position of the maxima only varies of a few Kelvin between the two polymorphs, the value of the nucleation rate at the maximum is significantly different by about four orders of magnitudes favoring the nucleation of the metastable I_α in agreement with its lower interfacial free energy. In the same figure, we compared the nucleation rates obtained from the CNT to the experimental values obtained by Andronis and Zografi[8]. It should be mentioned that one should be cautious about the nucleation rates from Andronis and Zografi[8] since the role of free surfaces remains unclear up to now. As already observed in several studies[23 94 37], although the overall bell-shaped of the nucleation rate is approximately well reproduced in the correct temperature domain, a major disagreement between the absolute value of the nucleation rate is obtained.

In the present study, nucleation rates predicted from simulation are different from those measured experimentally by more than eight decades at some temperatures despite the same version of the CNT employed and similar values of the interfacial free energy (see Table 1). The surprising large difference could originate from different factors. The most important is the physical parameter used to represent the effect of dynamics to the nucleation rate. The viscosity η is used by Andronis and Zografi[8] while the diffusivity D is used in the present work. Assuming the validity of the Stokes-Einstein (SE) equation, both η and D should be equivalent but, as reported in ref.[3], a breakdown of the SE relation is found in deeply supercooled situations of indomethacin. Using the fractional version of the SE equation ($T/D \sim \eta^{-\xi}$ with ≈ 0.78), Wu & Yu[3] were able to reanalyze the temperature dependence of the growth rate of indomethacin and have shown that diffusion actually controls crystal growth kinetics over a wide range of temperature. It is also clearly demonstrated in the present work (see growth rates prediction in Figure 6b) which confirms that diffusivity D instead of viscosity η better represents the effect of dynamics. Using the diffusivity D instead of η, the calculated nucleation rates obtained in the present study are much higher than those obtained by Andronis and Zografi. The second factor is the jump distance λ for a molecule at the surface of the crystal-liquid interface during the process of nuclei formation. In the Andronis and Zografi[8] work, $\lambda^3 = V_{unit\ cell}$ is assumed where $V_{unit\ cell}$ is the known volume of the crystalline cell. In the present work, $\lambda^3 = 1/n_{lq}$ is assumed where n_{lq} is the number density of the liquid state obtained from the MD simulations. As noted by Andronis and Zografi[8], the prefactor $A_N(T)$ (see equation 4) is clearly impacted by the choice of λ. Because the volume of the liquid is higher than the crystal one, the calculated nucleation rates ($\sim 1/\lambda^3$) obtained in the present study are higher than those obtained by Andronis and Zografi. The third factor is the small but clear discrepancy between the values of the interfacial free energy obtained by Andronis and Zografi[8] and in the present study (see Figure 5 and Table 1). The differences actually range from about 1 to 3 mJ/m^2. Although small, these differences may also significant impact the nucleation rate because of the mathematical form of the CNT equations. The obtained values of the interfacial free energy in the present work are always smaller than the values determined by Andronis and Zografi i.e. the nucleation are higher accordingly. The four and most complicated factor is the complex way the interfacial free energy is used in the CNT equation by Andronis and Zografi. Actually, two different interfacial free energies are used: one for the prefactor and one for the nucleation barrier. Indeed, in addition to the nucleation barrier (ΔG^*), the interfacial free energy is also present in the prefactor (Zeldovich factor). In Andronis and Zografi, the interfacial free energy is first assumed constant (see Figure

10 in ref. [8]) by plotting log(nucleation rate x η/T) vs $1/(T.\Delta G_v{}^2)$, 27 mJ/m^2 and 17 mJ/m2 are obtained. These values are then used to estimate the kinetic pre-factor. In Figure 11 in in ref. [8], the interfacial free energy becomes a temperature-dependent adjustable parameter but the value of the interfacial free energy in the kinetic pre-factor is kept constant (to the value previously determined). In ref. [8], for the I_α polymorph, both values are found similar: 17 mJ/m^2 (see figure 10 in ref. [8]) and between 16 to 17 mJ/m^2 (see Figure 11 in ref. [8]). So, the impact is quite limited. It it more important for the I_γ polymorph since larger differences are found: 27 mJ/m2 (see figure 10 in ref. [8]) and between 16 to 19 mJ/m2 (see Figure 11 in ref. [8]). For the CNT prefactor of the I_γ polymorph, the Andronis & Zografi interfacial free energy used is about 10 mJ/m^2 larger than in the present work. It is another contribution to the difference found between the two works concerning the nucleation rates. As a final remark, it could be also noted that it is also exist a difference between the experimental diffusion and the calculated/extrapolated diffusivity of about one order of magnitude. Increasing diffusivity by a factor 10 would obviously increase the calculated nucleation rate by a factor of 10 as well. The difference with respect to the nucleation rates determined by Andronis & Zografi would be even more marked. So, the differences in the experimental diffusion versus the calculated/extrapolated diffusivity do not seem to explain the difference in nucleation rates. The authors have tempted to recalculate nucleation rates using as much as possible the Andronis and Zografi approach described and the major discrepancy is clearly reduced (see inset in Figure 6a).

From the same set of parameters used to calculate the nucleation rate N, the growth rate G has been computed by the following equation [9]:

$$G = k \cdot A_G(T) \cdot f(T) \cdot \left[1 - exp\left(-\frac{\Delta G}{k_b T}\right)\right] \quad (5)$$

where k is a constant that does not depend on temperature, $A_G(T)$ (unit: m/s) is a parameter describing the molecular mobility and has been approximated by $\frac{D \cdot a}{\lambda^2}$ in the following where a is the average width of the crystal lattice spacing ($a \approx 1/{n_{cx}}^{1/3}$). The probability of attachment/detachment of molecules to the crystal nucleus is characterized by the last term in Eq. 5. The growth mechanism at the interface is defined by $f(T)$ which is a dimensionless function. In general, three main models of growth have been suggested [9]: normal, two-dimensional and screw dislocation growth. Each model of growth is defined by a specific form of the function $f(T)$. In this work, the growth rate were calculated using the three models $f(T)$ and compared to the experimental ones (see Figure 6b) obtained by Wu and Yu[3]. The model of growth which provides by far the best agreement between simulations and experiments is the normal mode growth model ($f \approx 1$) as suggested by Wu and Yu[3] in contrast with the two dimensional growth[3,8] model proposed by Andronis and Zografi.[8] The main difference between these two works actually originates from the description of the molecular mobility and its temperature dependence .i.e. the $A_G(T)$ term in Eq. 5. In Andronis and Zografi.[8], molecular mobility is described by $D \sim \eta^{-1}$ as predicted by the SE relation. In Wu and Yu[3], molecular mobility is described by $D \sim \eta^{-\xi}$ and thus a breakdown of the SE relation is considered. Since from the present numerical investigation the diffusion D is directly measured, it allows us to confirm the validity of the Wu and Yu[3] approach. To be perfectly clear, it should be mentioned that the viscosity-diffusivity breakdown cannot not be directly checked by computing viscosity $\eta(T)$ and diffusivity $D(T)$ separately as function of the temperature T from MD simulations. Indeed, because of the slow dynamics of Indomethacin compared to accessible MD simulations timescale, $D(T)$ and $\eta(T)$ cannot be computed in the deep undercooled regime at which the SE

is supposed to break. Actually, in the high temperature regime investigated from MD simulations (see Figure 2), the SE holds relatively well (see supplementary material Figure S3).

As shown in Figure 6b, computed values as function of the temperature qualitatively resemble the experimental growth rate of both polymorphs. The expected bell-curve of the growth rate G is obtained due to the respective increase and decrease of the thermodynamical driving force and the mobility upon cooling. The position of the maximum growth rate is shifted by about 20 K and the growth rate at the maximum is about two orders of magnitude higher compared to the experimental data. At higher undercooling, the agreement between simulation and experiment becomes very fair. It should be noted that the thermodynamical term in eq. 5 $[1 - exp(-\Delta G/k_b T)]$ only plays a significant role at very small undercoolings $\Delta T \approx 0$ and thus growth rates are mostly controlled by dynamics, .i.e diffusivitiy D, over a wide range of temperature as shown by Wu and Yu.[3] The two orders of magnitude discrepancy observed between simulations and experiments for growth rate (see Figure 6b) could be thus related at least partially to the one order of magnitude discrepancy found in diffusivity (see Figure 2) which is suspected to originate from the inability of the OPLS force field to reproduce dynamics with enough accuracy (see above). Furthermore, the nucleation and growth curves in Figure 6 do not significantly overlap which confirms that indomethacin is a good glass former. This behavior is well in line with experimental data[77,95] that showed that indomethacin exhibits a very low crystallization tendency during cooling and reheating. It should be mentioned that below T_g + 19 K, a sudden rise of growth near the glass transition temperature T_g is observed experimentally with a different mode of growth (see Interfacial free energy section). [3,96]

CONCLUSIONS

By means of molecular dynamics simulations, the crystallization tendency in the undercooled liquid state of the stable I_γ and metastable I_α indomethacin polymorphs have been studied. The crystalline state of both polymorphs, their liquid state, and their crystal-liquid interface have been simulated in order to extract the main physical parameters involved in the nucleation and growth processes: density, enthalpy, melting point, diffusivity and the crystal-liquid interfacial free energy as well as their temperature dependence. Most of these physical parameters were reproduced with a fair agreement with experimental data. The interfacial free energies at the melting temperature γ_m obtained by the capillary fluctuation method were found to be 27 $\pm$ 3 mJ/m^2 for I_γ and 22 $\pm$ 3 mJ/m^2 for I_α. The lower interfacial free energy corresponds to the metastable form. It follows the same trend as the melting entropy values well in line with the Ostwald rule of stage. Computed values of the interfacial free energies corrected by Turnbull-like temperature dependence are of the same order as data obtained experimentally from homogeneous nucleation measurements.[8] From this set of dynamical and thermodynamical physical parameters, the nucleation and growth rates were calculated. Predictions from the classical nucleation theory and different growth models (normal, two-dimension nucleation and screw dislocation) were tested. The overall bell-shaped of the nucleation rates and the temperature at which nucleation rates reach their maxima are relatively well reproduced. However, a major disagreement between simulation and experiment for the absolute value of the nucleation rate is obtained. Interestingly, this disagreement seems similar for both polymorphs α and γ suggesting that the origin of the discrepancies could be attributed to the kinetic pre-factor

rather than the nucleation barrier. Oppositely, for growth rates, the agreement between simulation and experiment is really fair considering the model used and their approximation and the normal growth model was found to reproduce the experimental crystallization tendency of both indomethacin polymorphs. This result confirms that growth in indomethacin is mostly controlled by dynamics over a wide temperature range. The overall separation between the nucleation and growth curves enables to discuss the good glass-forming ability of indomethacin.

From the present works, while the agreement of the computed growth rates with experimental values appears very fair, the prediction of the nucleation rates seems more problematic with discrepancies reaching several orders of magnitude. For future works, several improvements for the present approach related to nucleation could be considered: determination of the dependence on the crystalline face in interaction with the liquid and thus the anisotropy of the interfacial free energy, use of prediction of the nucleation rate from non-homogeneous nucleation or taking into account of the time-lag before attending the steady state nucleation.

ACKNOWLEDGMENTS

The authors acknowledge the use of the facilities of the CRI (Villeneuve d'Ascq, France) where some calculations were carried out. This project has received funding from the Interreg 2 Seas programme 2014-2020 co-funded by the European Regional Development Fund under subsidy contract 2S01-059_IMODE.

REFERENCES

1. Descamps M. 2016. Disordered Pharmaceutical Materials. ed.: Wiley-VCH Verlag.
2. Hancock BC, Zografi G 1996. Characteristics and Significance of the Amorphous State in Pharmaceutical Systems. Journal of Pharmaceutical Sciences 86:1-12.
3. Wu T, Yu L 2006. Origin of Enhanced Crystal Growth Kinetics near Tg Probed with Indomethacin Polymorphs. The Journal of Physical Chemistry B 110:15694-15699.
4. Deb B, Ghosh A 2011. Crystallization Kinetics in Selenium Molybdate Molecular Glasses. Europhysics Letters 95:26002.
5. Surov AO, Solanko KA, Bond AD, Perlovich GL, Bauer-Brandl A 2012. Crystallization and Polymorphism of Felodipine. Crystal Growth and Design 12:4022-4030.
6. Gunn E, Guzei IA, Cai T, Yu L 2012. Polymorphism of Nifedipine: Crystal Structure and Reversible Transition of the Metastable β Polymorph. Crystal Growth and Design 12:2037-2043.
7. Jackson KA 2002. The Interface Kinetics of Crystal Growth Processes. Interface Science 10:159–169.
8. Andronis V, Zografi G 2000. Crystal Nucleation and Growth of Indomethacin Polymorphs from the Amorphous State. Journal of Non-Crystalline Solids 271:236-248.
9. Gutzow I, Schmelzer JWP. 2013. The Vitreous State Thermodynamics, Structure, Rheology, and Crystallization. 2 ed., Berlin, Heidelberg: Springer
10. Debenedetti PG. 1996. Metastable Liquids: Concepts and Principles. ed., Princeton, New jersey: Princeton University Press.
11. Porter DA, Easterling KE. 1992. Phase Transformations in Metals and Alloys. ed., Boca Raton, U.S.A.: CRC Press.
12. Kirkpatrick RJ 1975. Crystal Growth from the Melt: A Review. American Mineralogist 60:798-614.
13. Woodruff DP. 1973. The Solid-Liquid Interface. ed., London, U.K.: Cambridge University Press.
14. Turnbull D 1950. Formation of Crystal Nuclei in Liquid Metals. Journal of Applied Physics 21:1022-1028.
15. Hoffman JD 1958. Thermodynamic Driving Force in Nucleation and Growth Processes. The Journal of Chemical Physics 29:1192-1193.
16. Becker SR, Poole PH, Starr FW 2006. Fractional Stokes-Einstein and Debye-Stokes-Einstein Relations in a Network-Forming Liquid. Physical Review Letters 97:055901.
17. Weil KG 1984. J. S. Rowlinson and B. Widom: Molecular Theory of Capillarity, Clarendon Press, Oxford 1982.. Berichte der Bunsengesellschaft für physikalische Chemie 88(6):586-586.
18. Wang J, Tang YW, Zeng XC 2006. Solid-Liquid Interfacial Free Energy of Water: A Molecular Dynamics Simulation Study. Journal of Chemical Theory and Computation 3:1494-1498.
19. Ocak Y, Akbulut S, Keslioglu K, Marasli N 2008. Solid-Liquid Interfacial Energy of Neopentylglycol. Journal of Colloid and Interface Science 320:555-562.
20. Jones DRH 1974. Review The Free Energies of Solid-Liquid Interfaces. Journal of materials science 9:1-17.
21. Glicksman ME, Vold CL 1969. Determination of Absolute Solid-Liquid Interfacial Free Energies in Metals. Acta Metallurgica 17:1-11.
22. Kang DH, Zhang H, Yoo H, Lee HH, Lee S, Lee GW, Lou H, Wang X, Cao Q, Zhang D, Jiang J 2014. Interfacial Free Energy Controlling Glass-Forming Ability of Cu-Zr Alloys. Scientific reports 4:5167.
23. Wu DT, Gránásy L, Spaepen F 2004. Nucleation and the Solid–Liquid Interfacial Free Energy. MRS Bulletin 29:945-950.
24. Roazas RE, Horbach J 2011. Capillary Wave Analysis of Rough Solid-Liquid Interfaces in Nickel. Europhysics Letters 93:26006.
25. Bai X, Li M 2006. Calculation of Solid-Liquid Interfacial Free Energy: A Classical Nucleation Theory Based Approach. J Chem Phys 124:124707.

26. Broughton JQ, Gilmer GH 1986. Molecular Dynamics Investigation of the Crystal-Fluid Interface. VI. Excess Surface Free Energies of Crystal-Liquid Systems. Journal of Chemical Physics 84:5759-5768.
27. Hoyt JJ, Asta M 2002. Atomistic Computation of Liquid Diffusivity, Solid-Liquid Interfacial Free Energy, and Kinetic Coefficient in Au and Ag. Phys Rev B 65:214106.
28. Hoyt JJ, Asta M, Karma A 2000. Method for Computing the Anisotropy of the Solid-Liquid Interfacial Free Energy. Physical Review Letters 86:5530.
29. Davidchack RL, Laird BB 2000. Direct Calculation of the Hard-Sphere Crystal/Melt Interfacial Free Energy. Physical Review Letters 85:4751-4754.
30. Davidchack RL, Laird BB 2003. Direct Calculation of the Crystal-Melt Interfacial Free Energies for Continuous Potentials: Application to the Lennard-Jones System. J Chem Phys 118:7651-7657.
31. Handel R, Davidchack RL, Anwar J, Brukhno AV 2008. Direct Calculation of Solid-Liquid Interfacial Free Energy for Molecular Systems: TIP4P Ice-Water Interface. Physical Review Letters 100:036104.
32. Davidchack RL, Morris JR, Laird BB 2006. The Anisotropic Hard-Sphere Crystal-Melt Interfacial Free Energy from Fluctuations. J Chem Phys 125:094710.
33. Amini M, Laird BB 2008. Crystal-Melt Interfacial Free Energy of Binary Hard Spheres from Capillary Fluctuations. Phys Rev E 78:144112.
34. Morris JR 2002. Complete Mapping of the Anisotropic Free Energy of the Crystal-Melt Interface in Al. Phys Rev B 66:144104.
35. Becker CA, Olmsted DL, Asta M, Hoyt JJ, Foiles SM 2009. Atomistic Simulations of Crystal-Melt Interfaces in a Model Binary Alloy: Interfacial Free Energies,Adsorption Coefficients, and Excess Entropy. Phys Rev B 79:054109.
36. Feng X, Laird BB 2006. Calculation of the Crystal-Melt Interfacial Free Energy of Succinonitrile From Molecular Simulation. The Journal of Chemical Physics 124:044707.
37. Gerges J, Affouard F 2015. Predictive Calculation of the Crystallization Tendency of Model Pharmaceuticals in the Supercooled State from Molecular Dynamics Simulations. J Phys Chem B 119:10768.
38. Reinhardt A, Doye JPK, Noya EG, Vega C 2012. Local Order Parameters for Use in Driving Homogeneous Ice Nucleation with All-Atom Models of Water. The Journal of Chemical Physics 137:194504.
39. Espinosa JR, Vega C, Sanz E 2014. The Mold Integration Method for the Calculation of the Crystal-Fluid Interfacial Free Energy from Simulations. J Chem Phys 141:134709.
40. Auer S, Frenkel D 2001. Prediction of absolute crystal-nucleation rate in hard-sphere colloids. Nature 409(6823):1020-1023.
41. Bai XM, Li M 2005. Differences between solid superheating and liquid supercooling. Journal of Chemical Physics 123(15).
42. Uberti SA, Ceriotti M, Lee PD, Finnnis MW 2010. Solid-Liquid Interface Free Energy Through Metadynamics Simulations. Phys Rev B 81:125416.
43. Fernández LA, Martín-Mayor V, Seoane B, Verrocchio P 2012. Equilibrium fluid-solid coexistence of hard spheres. Physical Review Letters 108:165701.
44. O'Brien M, McCauley J, Cohen E 1984. Indomethacin. Analytical Profiles of Drug Substances 13:211-238.
45. Hancock BC, Parcks M 1999. What is the true solubility advantage for amorphous pharmaceuticals? Pharmaceutical Research 17(4):397-404.
46. Jambhekar S, Casella R, Maher T 2003. The physicochemical characteristics and bioavailability of indomethacin from β-cyclodextrin, hydroxyethyl-β-cyclodextrin, and hydroxypropyl-β-cyclodextrin complexes. International Journal of Pharmaceutics 270:149-166.
47. Hamada Y, Nambu N, Nagai T 1975. Interactions of α- and β-Cyclodextrin with Several Non-Steroidal Antiinflammatory Drugs in Aqueous Solution. Chemical and Pharmaceutical Bulletin 23:1205-1211.

48. Swallen SF, Ediger MD 2011. Self-Diffusion of the Amorphous Pharmaceutical Indomethacin Near Tg. Soft Matter 7:10339-10344.
49. Aubrey-Medendorp C, Swadley MJ, Li T 2007. The polymorphism of indomethacin: an analysis by density functional theory calculations. Pharmaceutical Research 24(4):953-959.
50. Yoshioka M, Hancock BC, Zografi G 1994. Crystallization of Indomethacin from the amorphous state below and above its glass transition temperature. Journal of Pharmaceutical Sciences 83(12):1700-1705.
51. Legendre B, Feutelais Y 2004. Polymorphic and Thermodynamic Study of Indomethacin. Journal of Thermal Analysis and Calorimetry 76:255-264.
52. Johnson E 2002. The Elusive Liquid-Solid Interface. Science 296(5567):477-478.
53. Descamps M, Dudognon E 2014. Crystallization from the Amorphous State: Nucleation–Growth Decoupling, Polymorphism Interplay, and the Role of Interfaces. Journal of Pharmaceutical Sciences 103:2615–2628.
54. Ping W, Paraska WPD, Baker R, Harrowell P, Angell CA 2011. Molecular Engineering of the Glass Transition: Glass-Forming Ability across a Homologous Series of Cyclic Stilbenes. THE Journal of Physical Chemistry B 115:4696–4702.
55. Pedersen UR, Harrowell P 2006. Factors Contributing to the Glass-Forming Ability of a Simulated Molecular Liquid. THE Journal of Physical Chemistry B 115:14205-14209.
56. Todorov IT, Smith W. 2015. The DL_POLY_4 user manual, 4.07. ed., Daresbury, U.K.: STFC Daresbury Laboratory.
57. Jorgensen WL, Maxwell DS, TiradoRives J 1996. Development and testing of the OPLS all-atom force field on conformational energetics and properties of organic liquids. Journal of the American Chemical Society 118:11225-11236.
58. Caleman C, Van Maaren PJ, Hong M, Hub JS, Costa LT, Van der Spoel D 2011. Force Field Benchmark of Organic Liquids: Density, Enthalpy of Vaporization, Heat Capacities, Surface Tension, Isothermal Compressibility, Volumetric Expansion Coefficient, and Dielectric Constant. J Chem Theory Comput 8:61-74.
59. Jahn DA, Akinkunmi FO, Giovambattista N 2014. Effects of temperature on the properties of glycerol: A computer simulation study of five different force fields. Journal of Physical Chemistry B 118(38):11284-11294.
60. Sweere AJM, Fraaije JGEM 2017. Accuracy Test of the OPLS-AA Force Field for Calculating Free Energies of Mixing and Comparison with PAC-MAC. Journal of Chemical Theory and Computation 13(5):1911-1923.
61. Debenedetti PG, Truskett TM, Lewis CP, Stillinger FH 2003. Theory of supercooled liquids and glasses: Energy landscape and statistical geometry perspectives. Advances in Chemical Engineering 28:21-79.
62. Allen MP, Tildesley DJ. 1991. Computer Simulation of Liquids. ed., New York, U.S.: Oxford University Press.
63. Slavosh-Haghighi A, Thompson DL 2007. Melting Point Determination from Solid-Liquid Coexistence Initiated by Surface Melting. The Journal of Physical Chemistry C 111:7980–7985.
64. Belonoshko AB, Dubrovinsky LS 1995. Molecular Dynamics of Stishovite Melting. Geochimica et Cosmochimica Acta 59:1883-1889.
65. Mastny EA, De Pablo JJ 2007. Melting Line of the Lennard-Jones System, Infinite Size, and Full Potential. The Journal of Chemical Physics 127:104504.
66. Morris JR, Wang CZ, Ho KM, Chan CT 1993. Melting Line of Aluminum From Simulations of Coexisting Phases. Physical Review B 49:3109-3115.
67. Morris JR, Song X 2002. The Melting Lines of Model Systems Calculated From Coexistence Simulations. The Journal of Chemical Physics 116:9352-9358.
68. Feng X, Laird BB 2006. Calculation of the crystal-melt interfacial free energy of succinonitrile from molecular simulation. The Journal of Chemical Physics 124(4):044707.

69. Morris JR, Song X 2003. The Anisotropic Free Energy of the Lennard-Jones Crystal-Melt Interface. The Journal of Chemical Physics 119:3920-3925.
70. Benet J, MacDowell LG, Sanz E 2014. A study of the ice-water interface using the TIP4P/2005 water model. Physical Chemistry Chemical Physics 16:22159-22166.
71. Hadjittofis E, Isbell MA, Karde V, Varghese S, Ghoroi C, Heng JYY 2018. Influences of Crystal Anisotropy in Pharmaceutical Process Development. Pharmaceutical Research 35(5):100.
72. Steinhardt PJ, Nelson DR, Ronchetti M 1983. Bond-Orientational Order in Liquids and Glasses. Physical Review B 28:784-805.
73. Lechner W, Dellago C 2008. Accurate Determination of Crystal Structures Based on Averaged Local Bond Order Parameters. The Journal of Chemical Physics 129:114707.
74. Mickel W, Kapfer SC, Schröder-Turk GE, Mecke K 2013. Shortcomings of the Bond Orientational Order Parameters for the Analysis of Disordered Particulate Matter. The Journal of Chemical Physics 138:044501.
75. Chushak Y, Bartell LS 2000. Crystal Nucleation and Growth in Large Clusters of SeF_6 from Molecular Dynamics Simulations. The journal of physical Chemistry A 104:9328-9336.
76. Ngai KL. 2011. Relaxation and Diffusion in Complex Systems. ed., New York, U.S.A.: Springer Science & Business Media.
77. Baird JA, Santiago-Quinonez D, Rinaldi C, Taylor LS 2012. Role of Viscosity in Influencing the Glass-Forming Ability of Organic Molecules from the Undercooled Melt State. Pharmaceutical Research 29:271-284.
78. Mauro JC, Yue Y, Ellison AJ, Gupta PK, Allan DC 2009. Viscosity of Glass-Forming Liquids. Proceedings of the National Academy of Sciences 106:19780-19784.
79. Lunkenheimer P, Kastner S, Köhler M, Loidl A 2010. Temperature development of glassy α -relaxation dynamics determined by broadband dielectric spectroscopy. Physical Review E - Statistical, Nonlinear, and Soft Matter Physics 81(5).
80. Thompson CV, Spaepen F 1979. On the approximation of the free energy change on crystallization. Acta Metallurgica 27:1855-1859.
81. Marsac PJ, Konno H, Taylor LS 2006. A Comparison of the Physical Stability of Amorphous Felodipine and Nifedipine Systems. Pharmaceutical Research 23:2306-2316.
82. Gránásy L, Iglói F 1997. Comparison of experiments and modern theories of crystal nucleation. The journal of Chemical Physics 107:3634.
83. Peng LJ, Morris JR, Aga RS 2010. A parameter-free prediction of simulated crystal nucleation times in the Lennard-Jones system: From the steady-state nucleation to the transient time regime. The journal of Chemical Physics 133:084505.
84. Aga RS, Morris JR, Hoyt JJ, Mendelev M 2006. Quantitative Parameter-Free Prediction of simulated Crystal-Nucleation Times. Physical Review Letters 96:245701.
85. Baidakov VG, Tipeev AO 2012. Crystal nucleation and the solid–liquid interfacial free energy. The journal of Chemical Physics 136:074510.
86. Fokina VM, Zanottob ED, Yuritsync NS, Schmelzerd JWP 2006. Homogeneous crystal nucleation in silicate glasses: A 40 years perspective. Journal of Non-Crystalline Solids 352(26-27):2681–2714.
87. Baidakov VG, Protsenko SP, Tipeev AO 2013. Temperature dependence of the crystal-liquid interfacial free energy and the endpoint of the melting line. The journal of Chemical Physics 139(22):224703.
88. Wilson SR, Mendelev MI 2014. Dependence of solid–liquid interface free energy on liquid structure. Modelling and Simulation in Materials Science and Engineering 22(6):065004.
89. Kelton KF, Greer AL. 2010. Nucleation in Condensed Matter: Applications in Materials and Biology. ed.
90. Laird BB, Davidchack RL, Yang Y, Asta M 2009. Determination of the Solid-Liquid Interfacial Free Energy along a Coexistence Line by Gibbs-Cahn Integration. J Chem Phys 131:114110.

91. Spaepen F 1975. A Structural Model for The Solid-Liquid Interface in Monatomic Systems. Acta Metall 23:729.
92. Ostwald W 1897. Studien uber die Bildung und Umwandlung Fester Korper. Zeitschrift fur Physikalische Chemie:289-330.
93. Kashiev D. 2000. Nucleation: Basic Theory with Applocations. ed., Oxford: Butterworth-Heinemann.
94. Kelton KF, Ehrenreich H, Turnbull D. 1991. Solid State Physics. ed., Boston, U.S.A.: Academic Press.
95. Trasi NS, Baird JA, Kestur US, Taylor LS 2014. Factors Influencing Crystal Growth Rates from Undercooled Liquids of Pharmaceutical Compounds. Journal of Physical Chemistry B 118:9974−9982.
96. Hasebe M, Musumeci D, Powell CT, Cai T, Gunn EM, Yu L 2014. Fast surface crystal growth on organic glasses and its termination by the onset of fluidity. J Phys Chem B 118:7638−7646.

Table 1: Comparison between the experimental and the simulation data obtained for indomethacin I_α and I_γ crystal polymorphs. The exp and sim between parentheses represents the experimental and the simulated data respectively. ρ_{cx}, T_m, ΔH_m, ΔS_m and γ_m correspond to the crystal density determined at the respective T_m, the melting temperature, the melting enthalpy, the melting entropy and the interfacial free energy at the melting temperature respectively. Uncertainties of the interfacial free energy γ_m have been estimated from taking into consideration the uncertainties on the melting temperature about ± 10 K and the fitting procedure (see text).

Figure 1: Chemical structure of indomethacin $C_{19}H_{16}ClNO_4$.

Figure 2: Evolution of the shear viscosity η as a function of the inverse of temperature compared to the experimental data from Andronis et al. [8] and Bird et al.[77]. In inset, the calculated diffusivity a function of the inverse of temperature compared to the experimental data from Swallen et al. [48]. In inset, the solid line represents a fit using the MYEGA[78] equation $ln\left(\frac{1}{D}\right) = A_1 + \frac{A_2}{T} \cdot exp\left[\frac{A_3}{T}\right]$ with parameters A_1 = 17.70, A_2 = 463.98 K and A_3 = 956.02 K. The simulated shear viscosity η(T) is reported only for T ≥ 500K while the diffusivity D(T) is reported for T ≥ 400K. This difference originates from the poor statistics and convergence of the stress-stress autocorrelation function used to compute η(T) compared to the mean square displacement $< r^2(t) >$ used to compute the diffusivity D(T). The MYEGA fit was not performed on the viscosity data since some data at sufficient low temperatures are required to reproduce well the η vs T curvature. The validation of the Stokes-Einstein relation in the high temperature range probed by MD simulations is provided as supplementary material (see Figure S3).

Figure 3: a) Example of a simulation box used to obtain the interfacial stiffness of indomethacin I_α. The Y direction is normal to the interface while the X direction is along the interface. The system size is as follow: L_X =271.98 Å, L_Y = 240.48 Å and L_Z =36.05 Å (see text) where L_X, L_Y and L_Z are the dimensions of the whole simulation box along the X, Y and Z directions. b) An example of the evolution of the order parameter ϕ along the direction y orthogonal to the interface for a section $[x, x + \Delta]$. The solid line indicates the fitting using the following equation $\phi(y) = \frac{q_s+q_l}{2} + \frac{q_s-q_l}{2}\left[\tanh\left(\frac{y-h_1(x)}{\delta_1}\right) + \tanh\left(\frac{y-h_2(x)}{\delta_2}\right)\right]$ where $\delta_{1,2}$, q_s and q_l are the effective width of the interface, the average value of ϕ in the solid and liquid domain respectively. The subscripts 1 & 2 label the two interfaces created due to the boundary conditions. The zone corresponding to the interfaces has been indicated (δ_1 and δ_2).

Figure 4: The fluctuation spectrum $< |h(q)|^2 >$ of the interface height $h(x)$ for I_α and I_γ. The fits are represented by the solid lines (using Eq. 1) having a slope of -2. The fit was restricted to small values of q for which eq. 1 is valid[28].

Figure 5: The temperature dependent solid-liquid interfacial free energy $\gamma(T)$ (see Eq. 3) for the two crystal forms of indomethacin, I_γ (black solid line) and I_α polymorph (red dashed line). The solid-liquid interfacial free energy (including uncertainties ±3 mJ/m2) determined at the melting temperature using the capillary method is represented as opened symbols. Experimental data obtained by Andronis et Zografi[8] (filled symbols) are also included for comparison.

Figure 6: Evolution of the nucleation rates N (a) and growth rates G (b) rate as function of the temperature for the two investigated indomethacin polymorphs I_γ and I_α. See Eq. 4 and 5 in text. A comparison between experimental and numerical data is also given. The experimental data is taken from Andronis and Zografi[8] for the nucleation rates and Wu and Yu[3] for the growth rates. The growth rate results obtained by Andronis and Zografi[8] have been discarded since they are for

surface crystal growth, which are significantly enhanced relative to bulk crystal growth because of fast surface diffusion. One should be also cautious about the nucleation rates from Andronis and Zografi[8] since the role of free surfaces remains unclear. The role of free surfaces has since been clarified in.[96] Experimental glass transition temperature T_g and melting temperature T_m of the two indomethacin polymorphs are also indicated. Recalculation of the nucleation rates ((a) inset) using as much as possible the Andronis and Zografi[8] approach (dashed lines). The major discrepancy found between the nucleation rates determined in the present study (solid lines) and experimental values is clearly reduced. The plot of N as function of the undercooling ΔT also allows us minimizing the discrepancies that could be caused by the slight disagreement between the estimated and the experimental melting temperature Tm (see Table 1).

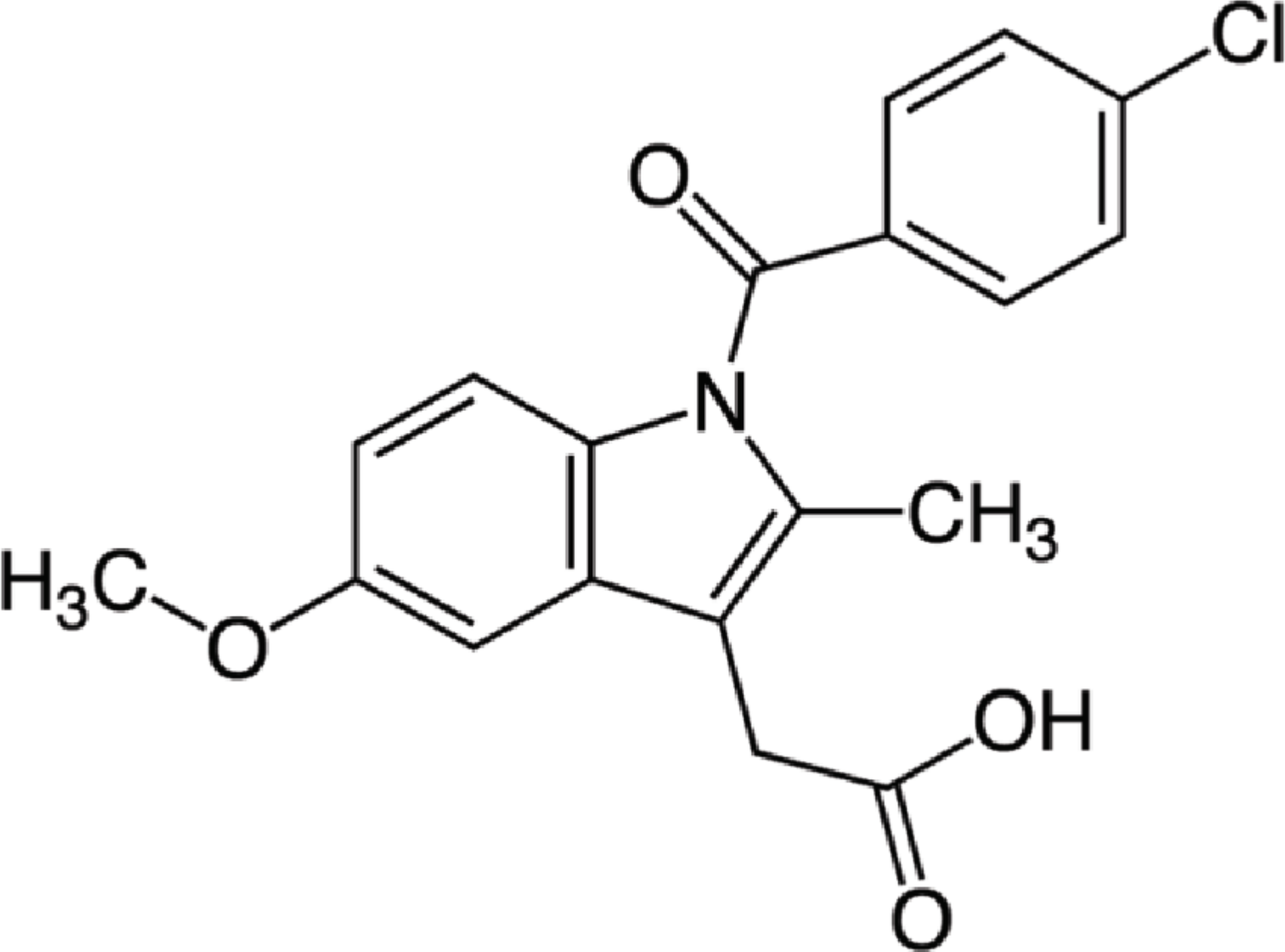
Cl
O
N
CH3
H3C
O
OH
O

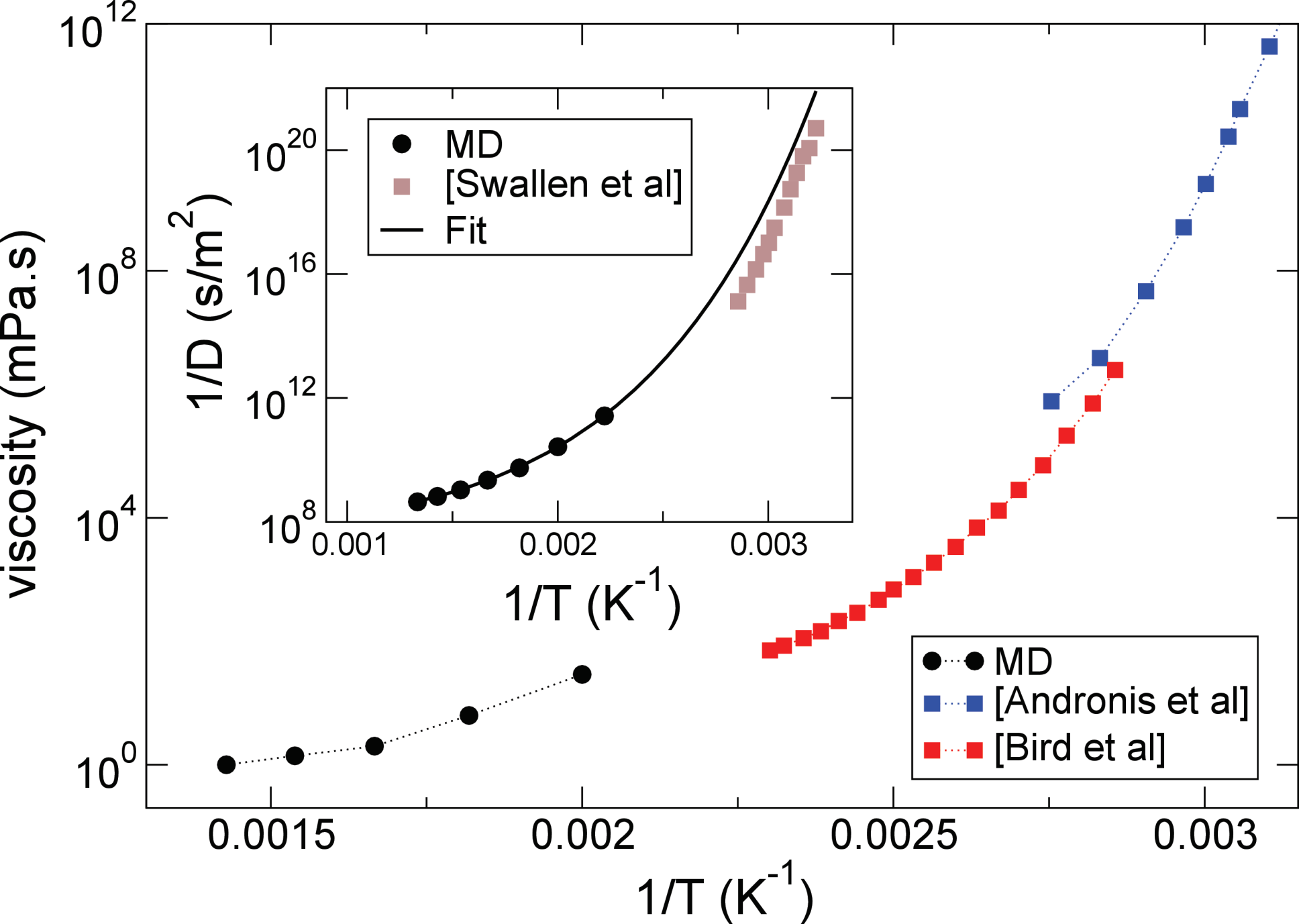
viscosity (mPa.s)
10^{12}
10^{8}
10^{4}
10^{0}
0.0015
0.002
0.0025
0.003
1/T (K^{-1})
MD
[Androns et al]
[Bird et al]
1/D (s/m^2)
10^{20}
10^{16}
10^{12}
10^{8}
0.001
0.002
0.003
1/T (K^{-1})
MD
[Swallen et al]
Fit

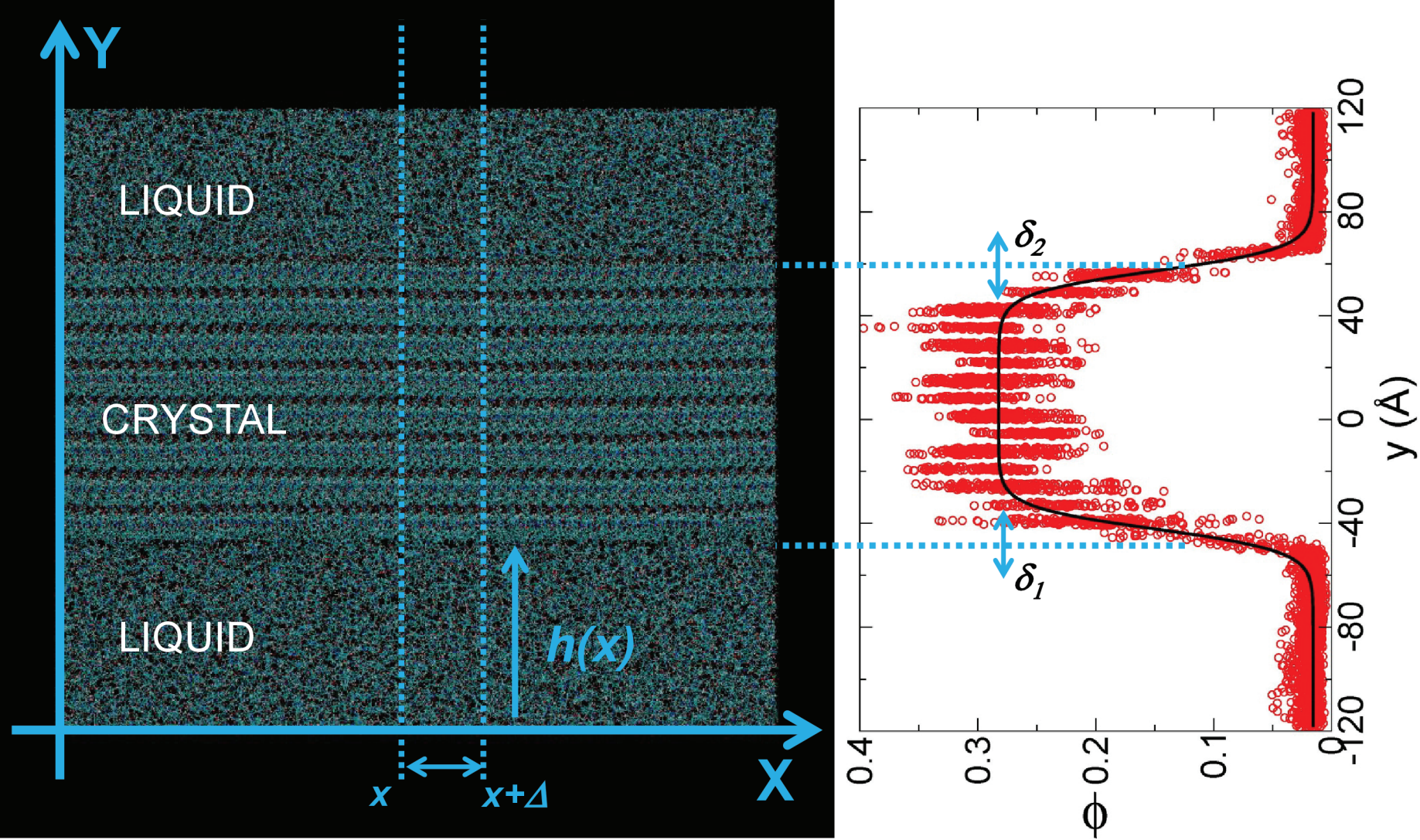
Y
LIQUID
CRYSTAL
LIQUID
h(x)
x
x+Δ
X
δ2
δ1
0.4
0.3
0.2
0.1
0
ϕ
120
80
40
0
-40
-80
-120
y (Å)

a)

b)

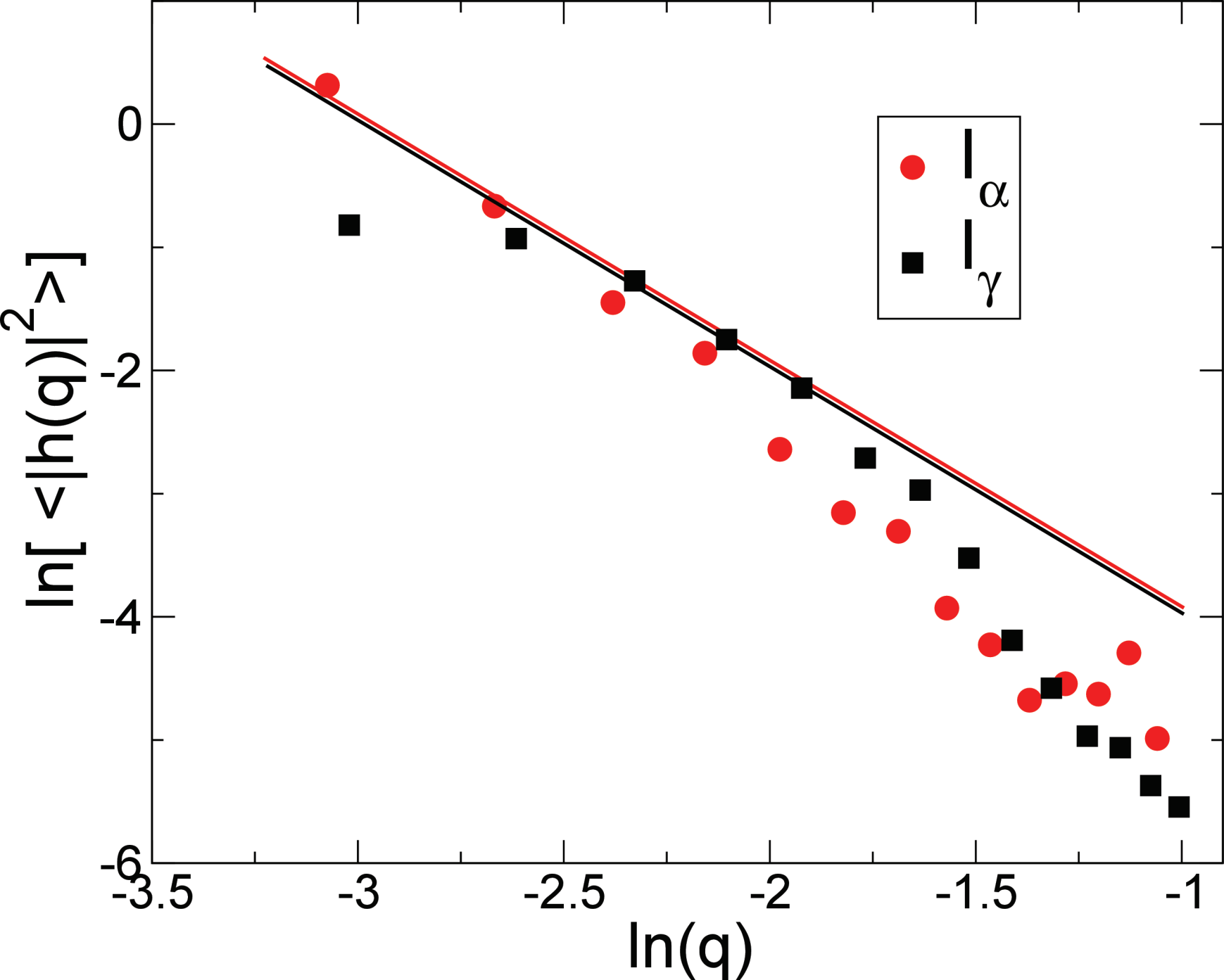
0
-2
-4
-6
-3.5
-3
-2.5
-2
-1.5
-1
ln[<|h(q)|^2>]
ln(q)
I α
I γ

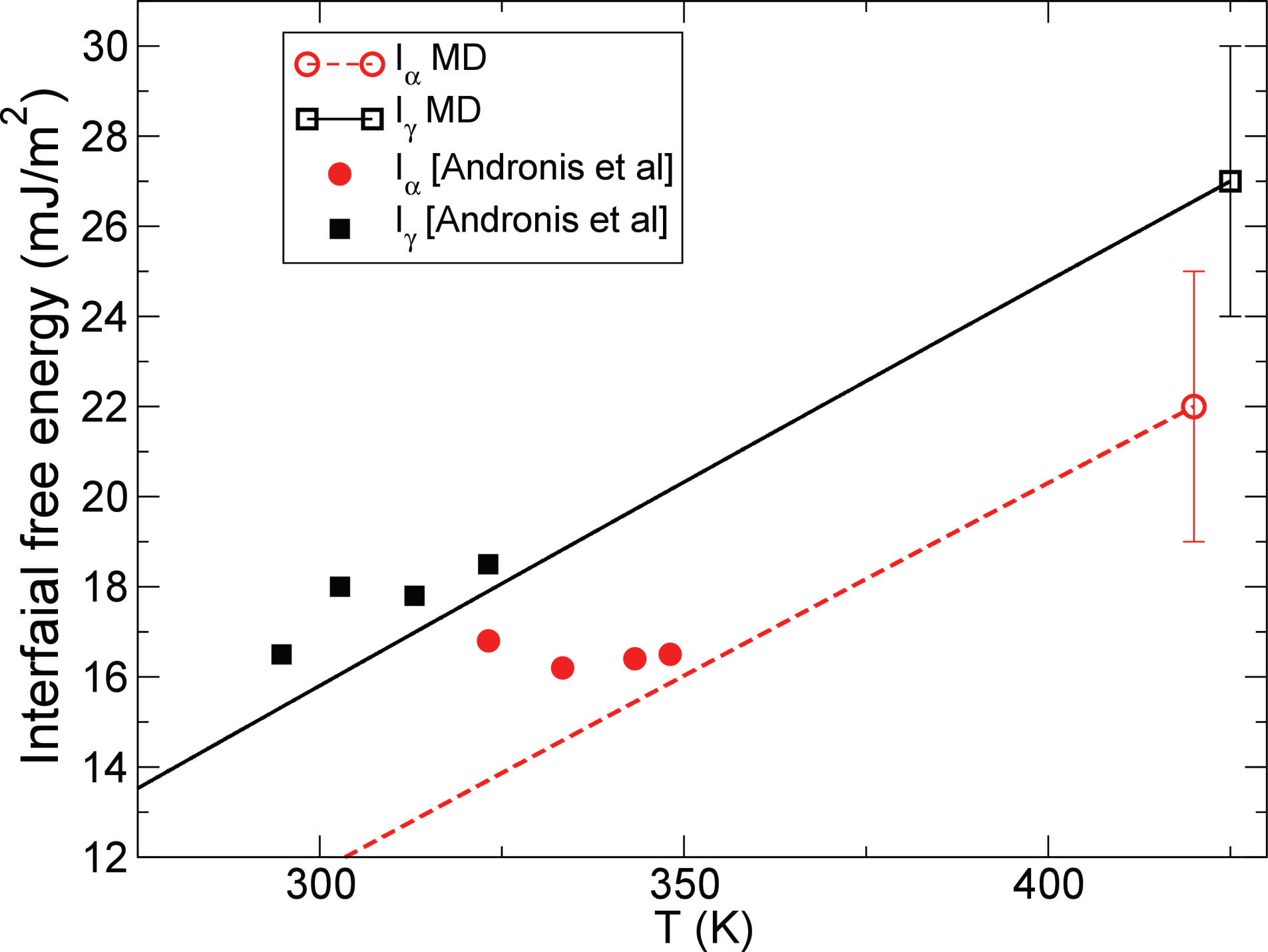
l_α MD
l_γ MD
l_α [Andronis et al]
l_γ [Andronis et al]
Interfaial free energy (mJ/m^2)
T (K)
30
28
26
24
22
20
18
16
14
12
300
350
400

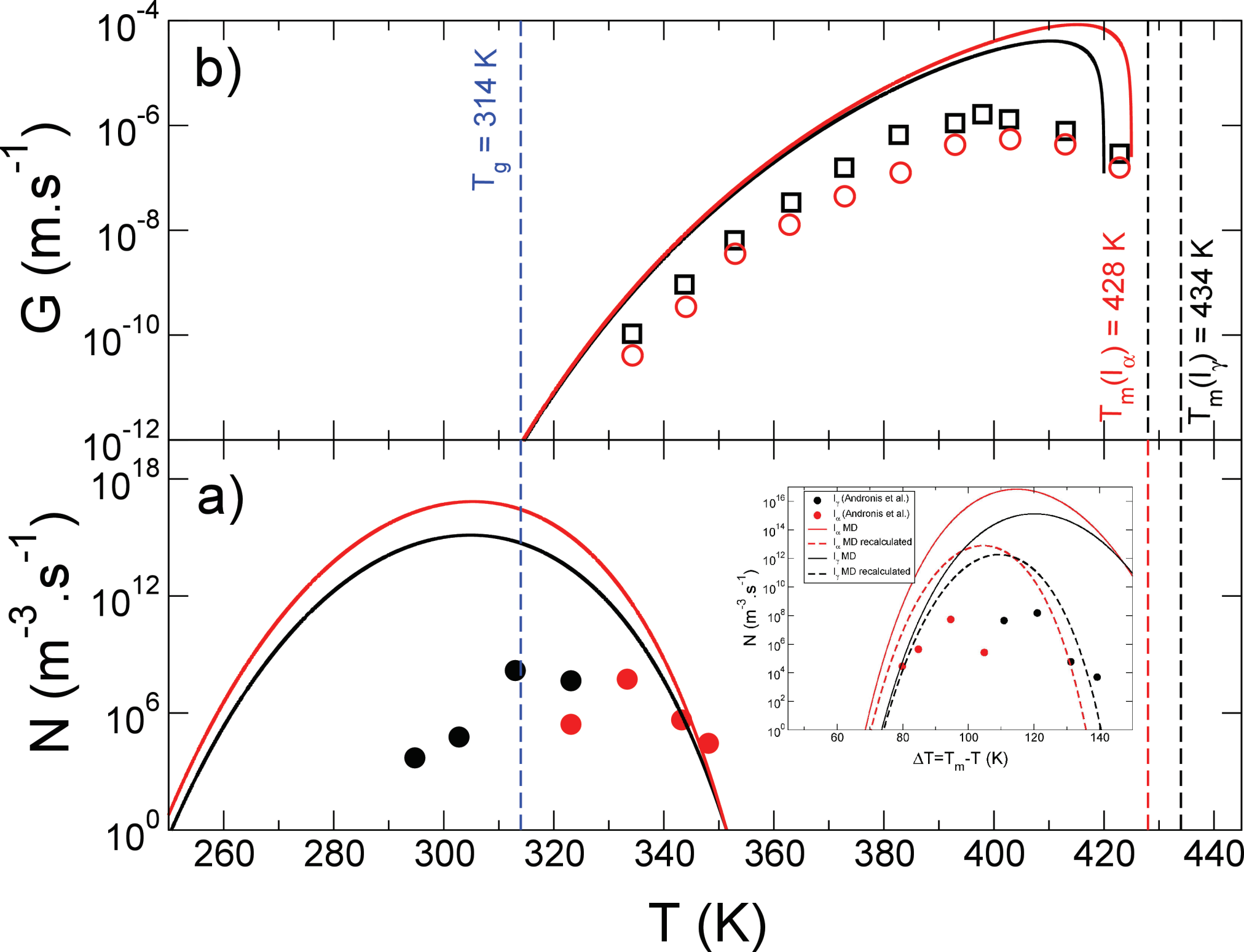
b)
a)
T_g = 314 K
$T_m(l_\alpha)$ = 428 K
$T_m(l_\gamma)$ = 434 K
G (m.s^{-1})
N (m^{-3}.s^{-1})
T (K)
l_γ (Andronis et al.)
l_α (Andronis et al.)
l_α MD
l_α MD recalculated
l_γ MD
l_γ MD recalculated
N (m^{-3}.s^{-1})
ΔT=T_m-T (K)

Table 1: Comparison between the experimental and the simulation data obtained for indomethacin I_α and I_γ crystal polymorphs. The exp and sim between parentheses represents the experimental and the simulated data respectively. ρ_{cx}, T_m, ΔH_m, ΔS_m and γ_m correspond to the crystal density determined at the respective T_m, the melting temperature, the melting enthalpy, the melting entropy and the interfacial free energy at the melting temperature respectively. Uncertainties of the interfacial free energy γ_m have been estimated from taking into consideration the uncertainties on the melting temperature about $\pm$10 K and the fitting procedure (see text).

Polymorph	ρ_{cx} (g/cm^3) (exp[52]/sim) at 300K	T_m (K) (exp[52]/sim)	ΔH_m (kJ/mol) (exp[52]/sim)	ΔS_m (J/(mol.K)) (exp[52]/sim)	γ_m (mJ/m^2) (exp[8]/sim)
I_α	1.40/1.35	428/420	32.5/28.6	75.9/68.1	16.2–16.8/ 22 ± 3
I_γ	1.38/1.32	434/ 425	39.3/39.4	90.6/92.7	16.5–18.5/ 27 ± 3